Supporting information

CoO Quantum Dots Anchored on Reduced Graphene Oxide Aerogels for Lithium Ion Storage

*Tianyu Zhu[a], Yan Wang[a, *], Yang Li[a], Rui Cai[a], Jianfang Zhang[a, b], Cuiping Yu[a], Jingjie Wu[b, c], Jiewu Cui[a, c], Yong Zhang[a, d], Pulickel M Ajayan[e], Yucheng Wu[a, c, f, *]*

[a]School of Materials Science and Engineering, Hefei University of Technology, Hefei, 230009, China

[b]Department of Chemical and Environmental Engineering, University of Cincinnati, Cincinnati, OH 45221, United States

[c]China International S&T Cooperation Base for Advanced Energy and Environmental Materials & Anhui Provincial International S&T Cooperation Base for Advanced Energy Materials, Hefei University of Technology, Hefei 230009, China

[d]Key Laboratory of Advanced Functional Materials and Devices of Anhui Province, Hefei 230009, China

[e]Department of Materials Science and Nano Engineering, Rice University, Houston, Texas 77005, United States

[f]Key Laboratory of Interface Science and Engineering in Advanced Materials of Ministry of Education, Taiyuan University of Technology, Taiyuan, 030024, China

***Corresponding authors:**

Email: stone@hfut.edu.cn (Dr. Yan Wang); ycwu@hfut.edu.cn (Prof. Yucheng Wu)

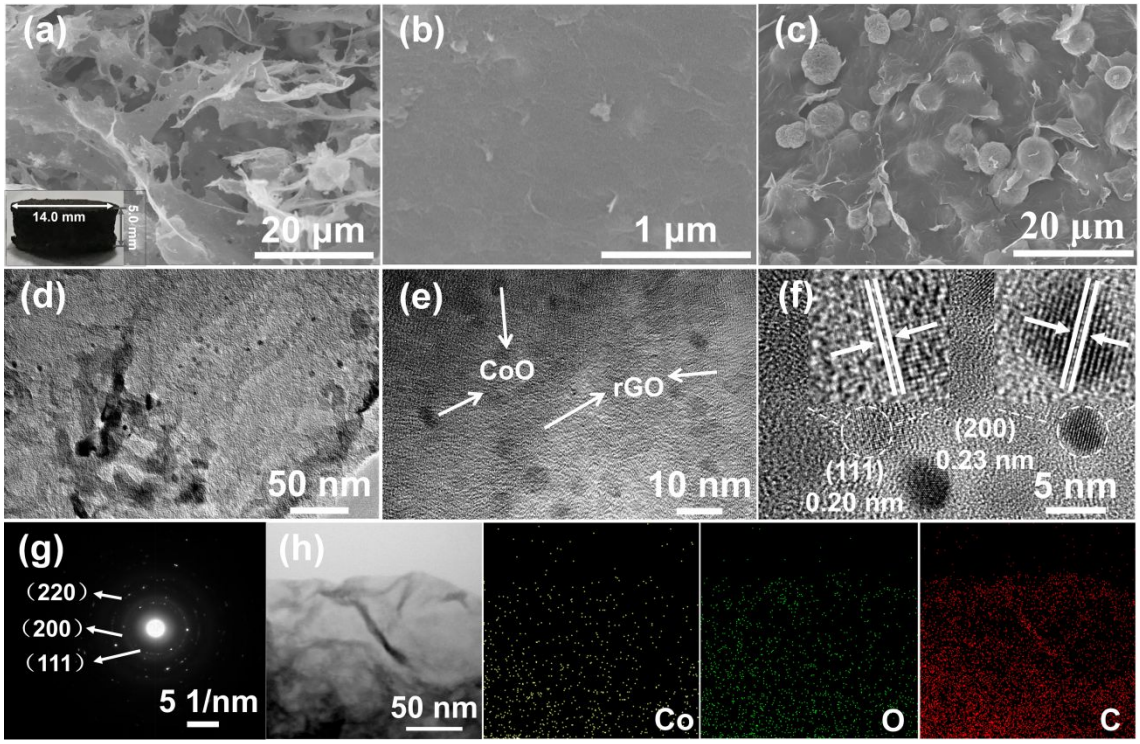

Figure S1. (a, b) FESEM images of CoO/rGO-2, the inset in (a) shows the optical photograph of the aerogel. (c) FESEM image of CoO/rGO-3. (d-h) TEM, HRTEM, SAED images and EDS mapping images of CoO/rGO-2.

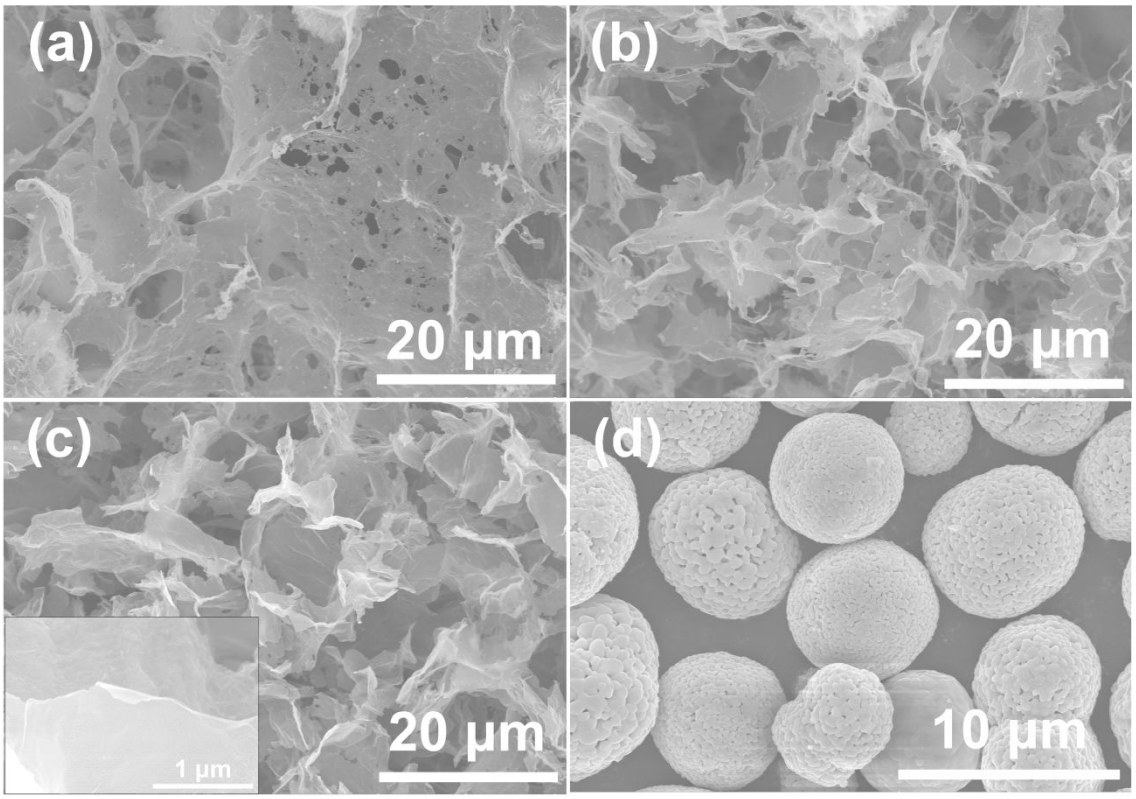

Figure S2. FESEM images of (a) the unannealed CoO/rGO-1 sample, (b) the unannealed CoO/rGO-2 sample, (c) the pure rGO and (d) the Co_3O_4 powders.

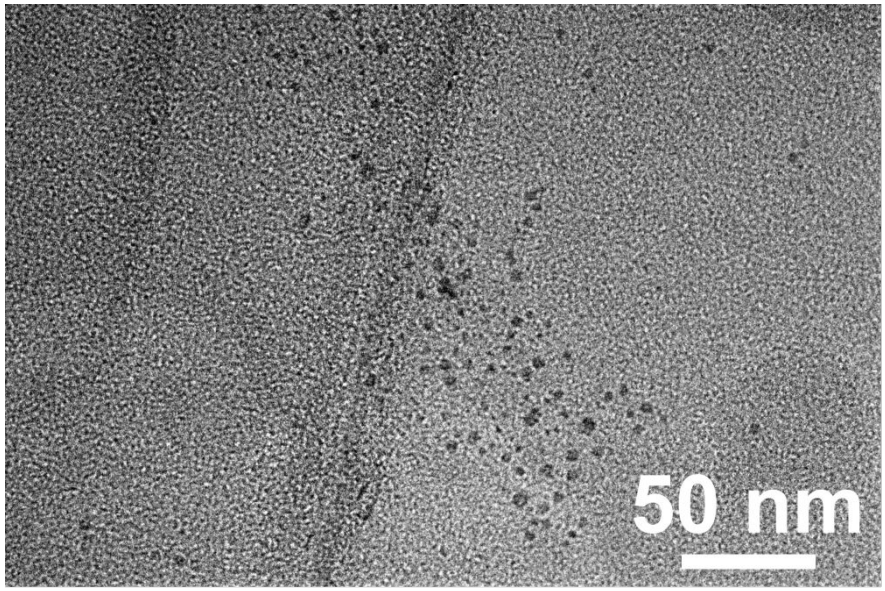

Figure S3. TEM image of Co_3O_4 quantum dots.

Table S1. Element content in samples CoO/rGO-1 and CoO/rGO-2 obtained by HRTEM characterization.

Element	CoO/rGO-1		CoO/rGO-2	
	Weight percentage (%)	Atomic percentage (%)	Weight percentage (%)	Atomic percentage (%)
C	68.32	84.52	80.69	88.14
O	11.07	10.28	12.66	10.38
Co	20.61	5.20	6.66	1.48
Total	100.00		100.00	

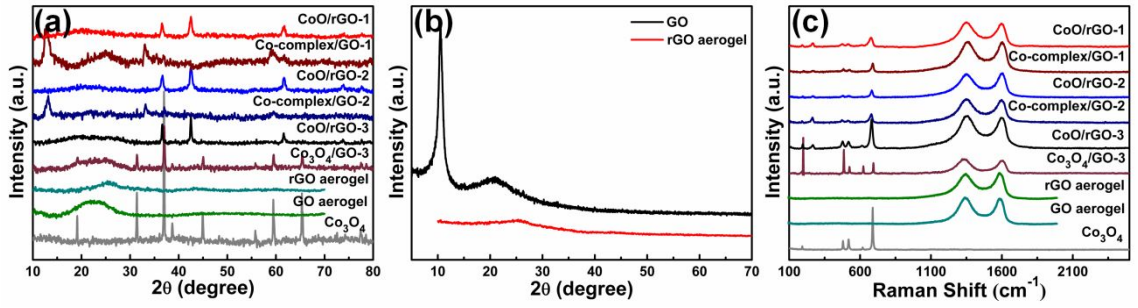

Figure S4. (a) XRD patterns and (c) Raman spectra of the CoO/rGO-1, CoO/rGO-2, CoO/rGO-3 samples and their intermediates, (b) XRD patterns of graphite oxide and rGO aerogel.

Table S2. Peak position (cm^{-1}) and the intensity ratio of D-band to G-band (I_D/I_G) of GO, rGO and CoO/rGO in Raman spectra.

Sample	Raman Shift (cm^{-1}) and I_D/I_G								
	Peak 1	Peak 2	Peak 3	Peak 4	Peak 5	Peak 6	Peak 7	Peak 8	I_D/I_G
GO							1354.4	1598.5	1.04
rGO							1356.0	1598.5	0.94
CoO/rGO-1	192.2	266.5	476.6	517.0	612.9	678.5	1352.9	1600.1	1.05
CoO/rGO-2	196.7	267.2	479.2	521.3	615.3	682.7	1352.0	1602.3	0.97
CoO/rGO-3	195.9	266.5	476.6	518.8	614.6	681.9	1352.9	1601.7	1.07

TG curves analysis

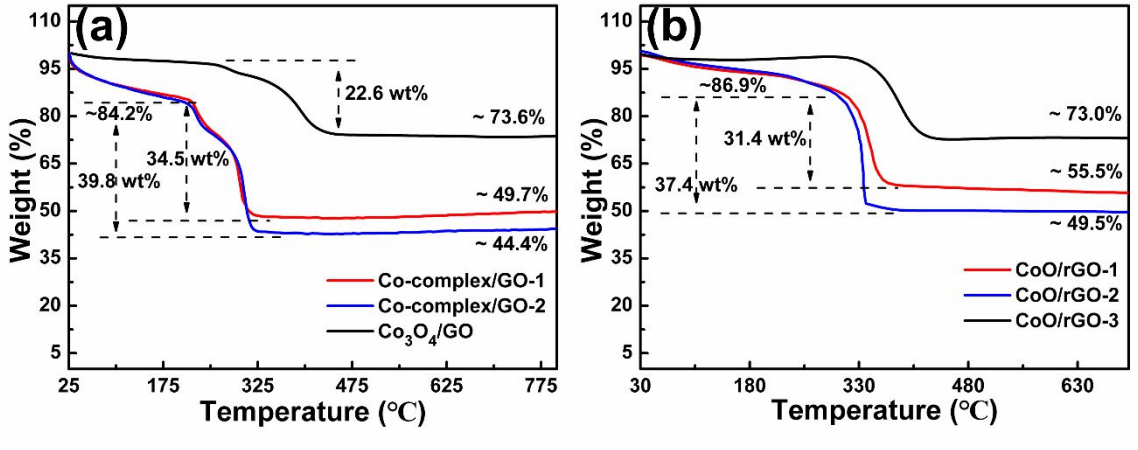

Figure S5. TG curves of CoO/rGO (a) before and (b) after heat treatment in Ar atmosphere.

Thermogravimetry/differentiate thermogravimetry analyses (TGA/DTG) (Figure S5) were performed on Co-complex/GO-1 and Co-complex/GO-2 as a reference to prepare the sample CoO/rGO-3. For the CoO/rGO aerogel before the heat treatment (Co-complex/GO-1 and Co-complex/GO-2), the curves show obvious mass loss at 25-200 ℃, 200-250 ℃ and 250-300 ℃ due to the evaporation of adsorbed H_2O, conversion of cobalt compounds and decomposition of oxygen-containing functional groups.[1-3] Stable Co_3O_4 was basically formed at 300 ℃, and the combustion decomposition of GO was basically completed. The product reached a stable level after 350 ℃. The TG curve of Co_3O_4/GO-3 shows that the mass loss mainly occurs at 270-440 °C. The content of cobalt oxide in the Co-complex/GO-1, Co-complex/GO-2 and Co_3O_4/GO-3 are 49.7 wt%, 44.4 wt% and 73.6 wt%, respectively.

The TG curves of the sample after heat treatment in Ar atmosphere are shown in Figure S5b, The mass content of rGO in the CoO/rGO-1, CoO/rGO-2 and CoO/rGO-3 are about 31.4 wt%, 37.4 wt% and 27.0 wt%, respectively. The weight loss from 30 to 200 ℃ is ascribed to the elimination of the absorbed H_2O, and the fast weight loss is due to the carbon

combustion.[3] The TG results further prove the extra CoO contained in CoO/rGO-1 than CoO/rGO-2.

The test results of the electrochemical performance of the CoO/rGO anodes show that the CoO/rGO-1 anode has the best rate capability and cycle life. This is related to the metal oxide QDs rich in active materials. Generally, the more metal oxides content, the higher its specific capacity in metal oxides/rGO composites, because the main contribution of metal oxides in composites is to provide high theoretical capacity. However, in our work, the CoO/rGO-3 anode with more cobalt oxide has the lowest specific capacity, indicating that the decisive factor for good electrochemical performance is not the high content of metal oxide, but the existence of metal oxide particles. The reason why CoO/rGO-1 and CoO/rGO-2 anodes have better electrochemical performance is because the small-sized nanoparticles in the active material play an important role. The CoO/rGO-1, which is rich in CoO QDs, has more prominent performance advantages.

Table S3. Average discharge specific capacity (mA h g^{-1}) at various current densities (A g^{-1}) for CoO/rGO.

Sample	Average discharge specific capacity (mA h g^{-1})						
	0.1 A g^{-1}	0.2 A g^{-1}	0.5 A g^{-1}	1.0 A g^{-1}	2.0 A g^{-1}	5.0 A g^{-1}	0.1 A g^{-1}
CoO/rGO-1	979.0	1043.3	1066.1	1058.4	1016.7	874.4	1389.7
CoO/rGO-2	816.0	866.2	880.1	871.3	834.3	727.8	1147.1
CoO/rGO-3	731.5	714.8	658.4	592.6	502.7	353.8	758.8

Table S4. Initial/final discharge specific capacity (mA h g^{-1}) and final Coulombic efficiency (%) of discharge-charge cycling at various current densities (A g^{-1}) for CoO/rGO.

Sample	Initial/final discharge specific capacity (mA h g^{-1}) (final Coulombic efficiency (%))		
	0.1 A g^{-1} (30 cycles)	0.5 A g^{-1} (100 cycles)	1 A g^{-1} (700 cycles)
CoO/rGO-1	960.9/1303.7 (95.8)	1128.7/1453.9 (97.2)	1018.2/726.1 (100.0)
CoO/rGO-2	815.9/1072.6 (96.4)	809.3/539.6 (99.1)	349.8/273.1 (100.0)
CoO/rGO-3	727.9/765.8 (97.4)	611.1/424.0 (98.6)	297.7/331.3 (99.8)(300 cycles)

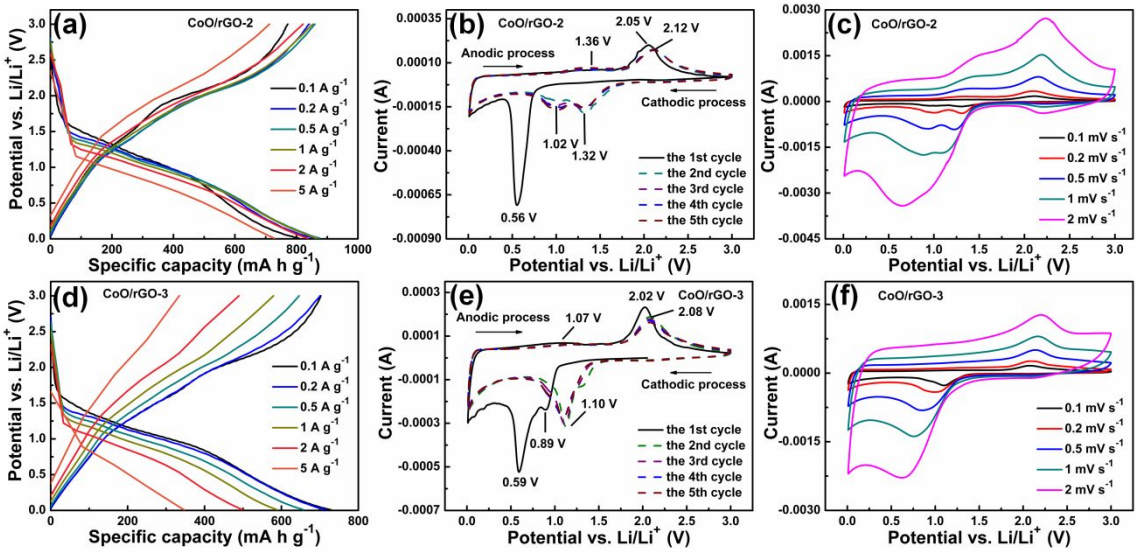

Figure S6. Galvanostatic discharge/charge profiles at varies current densities of (a) CoO/rGO-2 and (d) CoO/rGO-3, CV curves measured at 0.1 mV s^{-1} of (b) CoO/rGO-2 and (e) CoO/rGO-3, CV curves at different scan rates of (c) CoO/rGO-2 and (f) CoO/rGO-3.

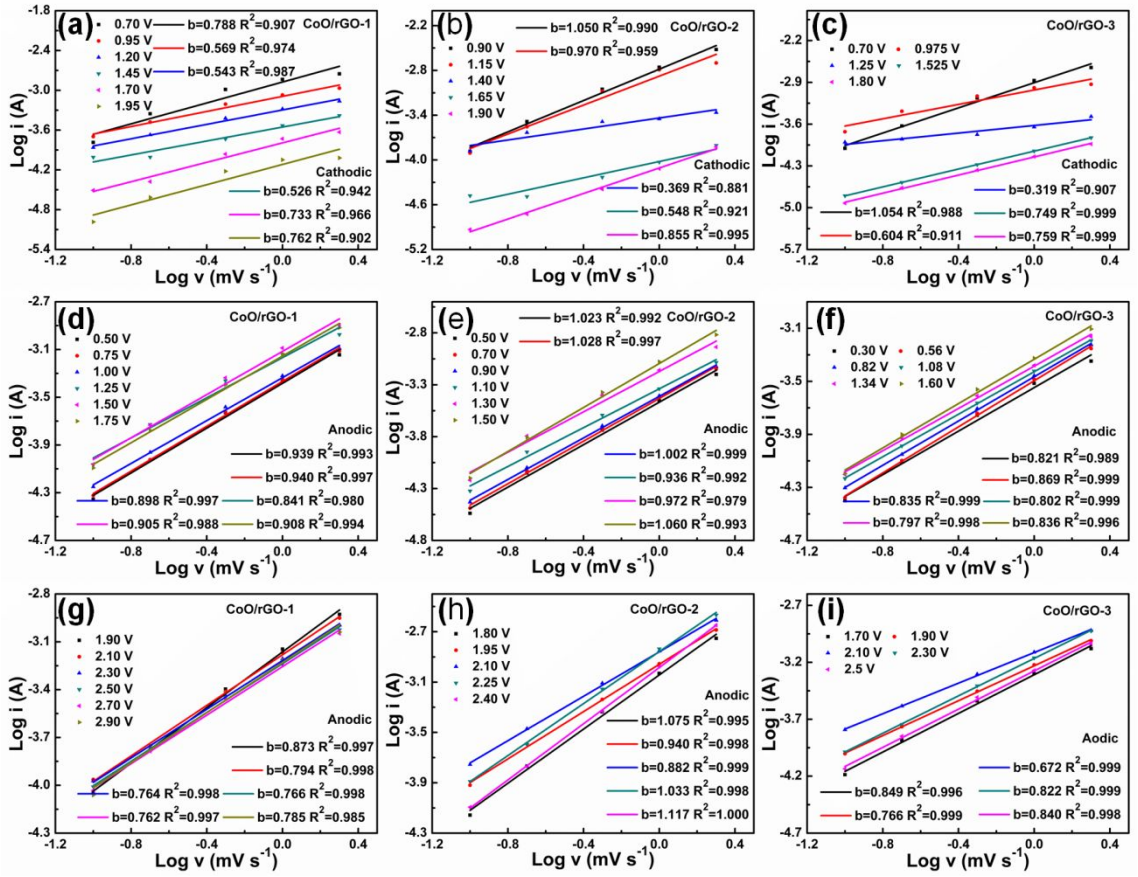

Figure S7. The linear relation of logarithm of the current (*i*) and scan rate (*v*) at varies potentials for (a, d, g) CoO/rGO-1, (b, e, h) CoO/rGO-2 and (c, f, i) CoO/rGO-3 anodes.

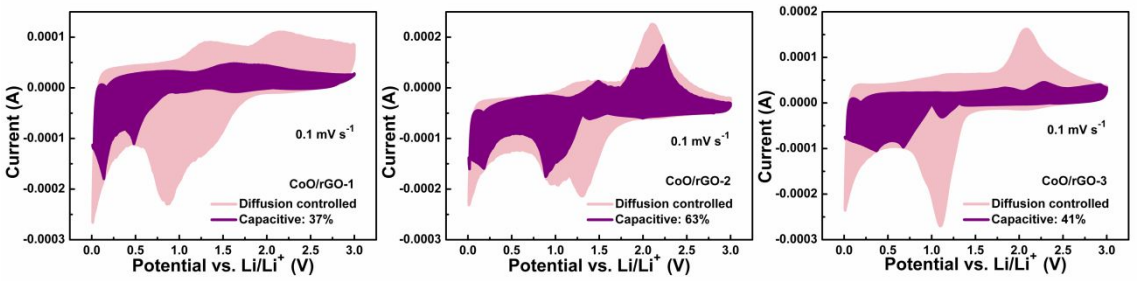

Figure S8. Capacitance-controlled capacity contribution (purple area) of (a) CoO/rGO-1, (b) CoO/rGO-2 and (c) CoO/rGO-3 anodes at 0.1 mV s^{-1}.

Table S5. Fitted Impedance Values of EIS for CoO/rGO-1, CoO/rGO-2 and CoO/rGO-3.

Sample	R_s (Ω)	R_f (Ω)	R_{ct} (Ω)	Z_w (Ω)
CoO/rGO-1	5.2	2.3	41.0	45.0
CoO/rGO-2	4.6	2.5	70.6	65.9
CoO/rGO-3	4.5	9.1	97.0	128.1

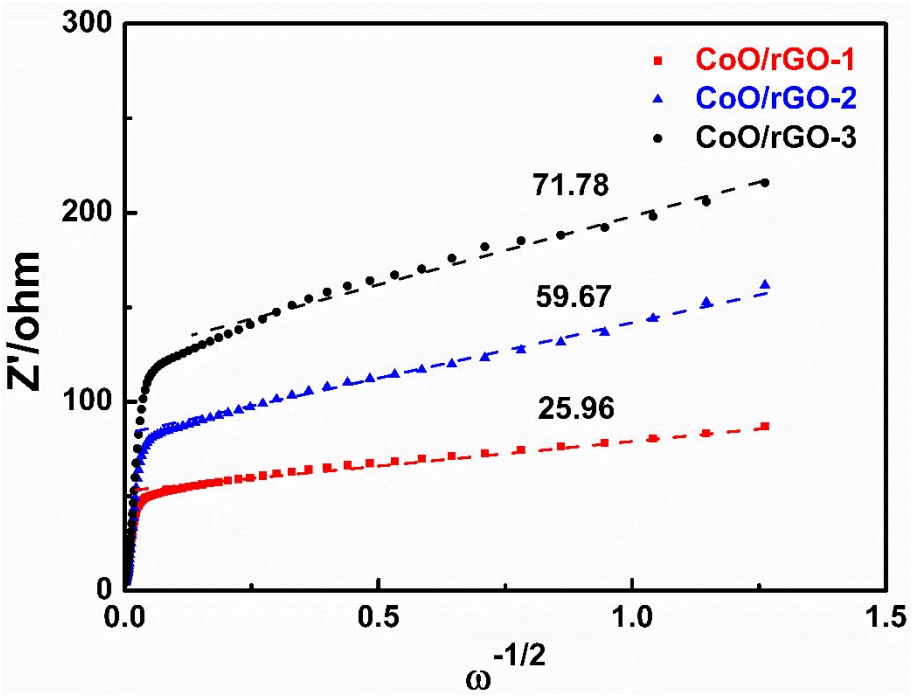

Figure S9. Linear Warburg impedance diagram of the CoO/rGO anodes.

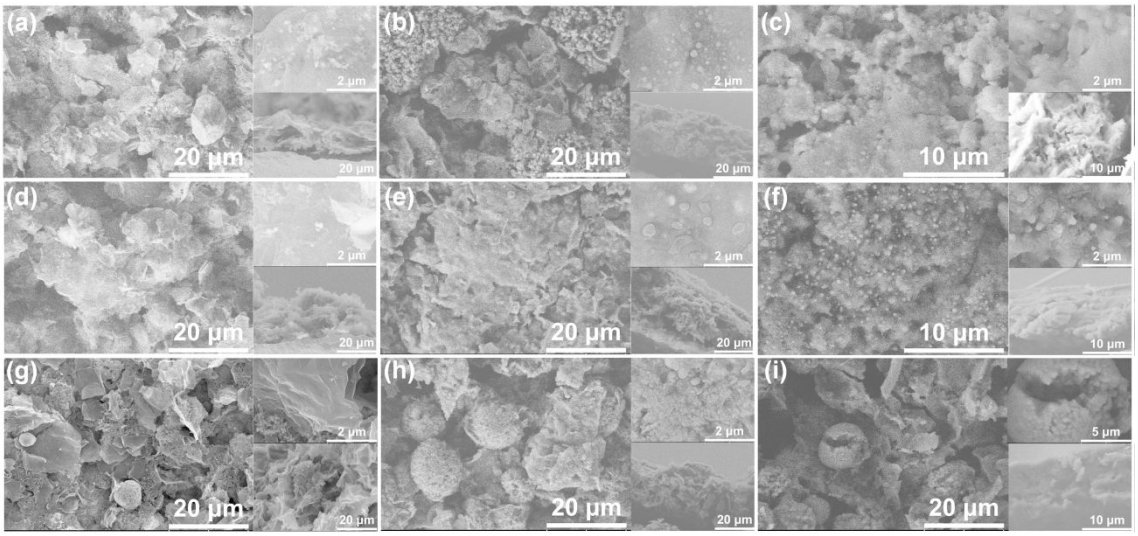

Figure S10. SEM images of the CoO/rGO anodes before and after cycling. (a) CoO/rGO-1, (d) CoO/rGO-2 and (g) CoO/rGO-3 anodes without electrochemical cycling. (b) CoO/rGO-1, (e) CoO/rGO-2 and (h) CoO/rGO-3 anodes after 5.5 cycles. (c) CoO/rGO-1, (f) CoO/rGO-2 and (i) CoO/rGO-3 anodes after activation of different cycles (the cross-sectional view is in the lower right corner).

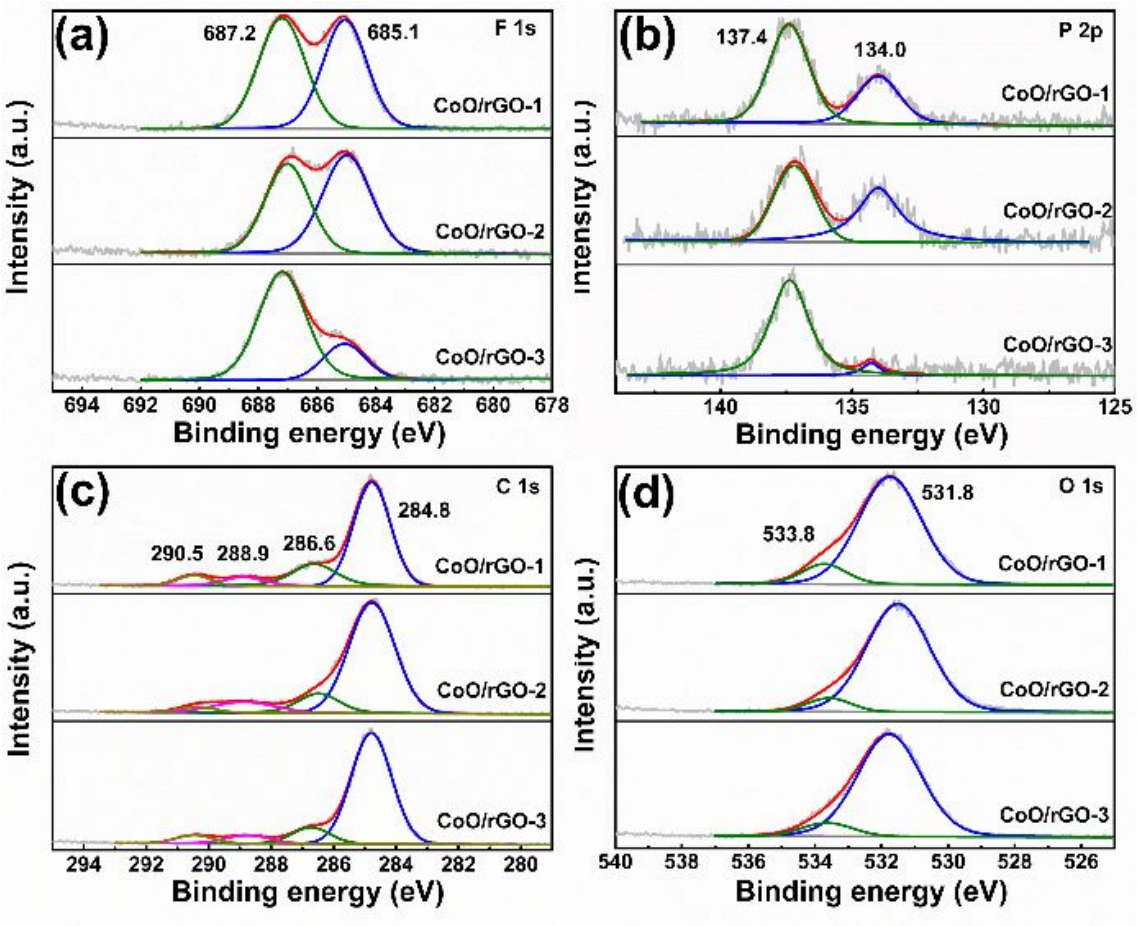

Figure S11. XPS spectra of (a) F 1s, (b) P 2p, (c) C 1s and (d) O 1s of CoO/rGO anodes after cycling at 0.1 A g^{-1}.

Table S6. Comparison of electrochemical performance for CoO/rGO composites prepared by different methods.

Materials	Synthesis method	Reversible capacity mA h g^{-1} (A g^{-1})	Cycling performance mA h g^{-1} (cycle, A g^{-1})	Ref.
CoO QDs/rGO	Ultrasonic fracturing combined with solvothermal	911.6 (1^{st} charge, 0.1), 1016.7 (2.0)	726.1 (700th, 1.0)	This work
CoO nanoparticles/rGO	Solvothermal method followed by a heating treatment	899 (1^{st} charge, 0.1), 602 (2.0)	1309 (100th, 0.1)	1
CoO-graphene hydrogel	Hydrothermal	984 (1^{st} charge, 0.1), 300 (1.6)	1010 (100th, 0.1)	4
CoO nanoparticles /graphene	Electrostatic self-assembly	722 (1^{st} charge, 0.1), 397 (2.0)	707 (1000th, 1.0)	5
CoO nanoparticles/rGO	Hydrothermal and heat treatment	826 (1^{st} charge, 0.2), 543.8 (1.6)	962.9 (80th, 0.2)	6
CoO/graphene	Mixing, centrifugation, hydrothermal and sintering	678 (1^{st} charge, 0.1), 450 (3.0)	604 (5000th, 1.0)	7
CoO quantum dots/graphene	Mixing and heat treatment	980 (1^{st} charge, 0.05), 1008 (1.0)	1592 (50th, 0.05)	8

REFERENCES

(1) Cao, L.; Kang, Q.; Li, J.; Huang, J.; Cheng, Y. Assembly control of CoO/reduced graphene oxide composites for their enhanced lithium storage behavior. *Appl. Surf. Sci.***2018,** *455*, 96-105, DOI: 10.1016/j.apsusc.2018.05.143.

(2) Wang, Y.; Liu, P.; Zhu, K.; Wang, J.; Yan, K.; Liu, J. One-step fabrication of in situ carbon-coated $NiCo_2O_4$@C bilayered hybrid nanostructural arrays as free-standing anode for high-performance lithium-ion batteries. *Electrochim. Acta* **2018,** *273*, 1-9, DOI: 10.1016/j.electacta.2018.04.023.

(3) Sun, B.; Lou, S.; Zheng, W.; Qian, Z.; Cui, C.; Zuo, P.; Du, C.; Xie, J.; Wang, J.; Yin, G. Synergistic engineering of defects and architecture in Co_3O_4@C nanosheets toward Li/Na ion batteries with enhanced pseudocapacitances. *Nano Energy* **2020,** *78*, 105366, DOI: 10.1016/j.nanoen.2020.105366.

(4) Binitha, G.; Ashish, A. G.; Ramasubramonian, D.; Manikandan, P.; Shaijumon, M. M. 3D Interconnected Networks of Graphene and Flower-Like Cobalt Oxide Microstructures with Improved Lithium Storage. *Adv. Mater. Inter.* **2016,** *3* (1), 1500419, DOI: 10.1002/admi.201500419.

(5) Prabakar, S. J. R.; Babu, R. S.; Oh, M.; Lah, M. S.; Han, S. C.; Jeong, J.; Pyo, M. Dense CoO/graphene stacks via self-assembly for improved reversibility as high performance anode in lithium ion batteries. *J. Power Sources* **2014,** *272*, 1037-1045, DOI: 10.1016/j.jpowsour.2014.09.044.

(6) Zhang, M.; Wang, Y.; Jia, M. Three-Dimensional Reduced Graphene Oxides Hydrogel Anchored with Ultrafine CoO Nanoparticles as Anode for Lithium Ion Batteries. *Electrochim.*

Acta **2014,** *129*, 425-432, DOI: 10.1016/j.electacta.2014.02.097.

(7) Huang, X.-l.; Wang, R.-z.; Xu, D.; Wang, Z.-l.; Wang, H.-g.; Xu, J.-j.; Wu, Z.; Liu, Q.-c.; Zhang, Y.; Zhang, X.-b. Homogeneous CoO on Graphene for Binder-Free and Ultralong-Life Lithium Ion Batteries. *Adv. Funct. Mater.* **2013,** *23* (35), 4345-4353, DOI: 10.1002/adfm.201203777.

(8) Peng, C.; Chen, B.; Qin, Y.; Yang, S.; Li, C.; Zuo, Y.; Liu, S.; Yang, J. Facile Ultrasonic Synthesis of CoO Quantum Dot/Graphene Nanosheet Composites with High Lithium Storage Capacity. *ACS NANO* **2012,** *6* (2), 1074-1081.